Biochemistry

 Volume 42, Number 20 May 27, 2003

Accelerated Publications

Structure of Frataxin Iron Cores: An X-ray Absorption Spectroscopic Study†

Helen Nichol,*,‡ Oleksandr Gakh,§ Heather A. O'Neill,§ Ingrid J. Pickering,|| Grazia Isaya,*,§ and Graham N. George||

Department of Anatomy and Cell Biology, University of Saskatchewan, Saskatoon, Saskatchewan, Canada S7N 5E5, Departments of Pediatric and Adolescent Medicine and of Biochemistry and Molecular Biology, Mayo Clinic and Foundation, Rochester, Minnesota 55905, and Stanford Synchrotron Radiation Laboratory, Stanford Linear Accelerator Center, Menlo Park, California 94025

Received October 17, 2002; Revised Manuscript Received March 13, 2003

ABSTRACT: X-ray absorption spectroscopy at the iron K-edge indicates that the iron cores of human and yeast frataxin polymers assembled *in vitro* are identical to each other and are similar but not identical to ferritin cores. Both frataxin polymers contain ferrihydrite, a biomineral composed of ferric oxide/hydroxide octahedra. The ferrihydrite in frataxin is less ordered than iron cores of horse spleen ferritin, having fewer face-sharing Fe−Fe interactions but similar double corner-sharing interactions. The extended X-ray absorption fine structure (EXAFS) analysis agrees with previous electron microscopy data showing that frataxin cores are composed of very small ferrihydrite crystallites.

The iron storage protein ferritin plays a key role in iron homeostasis and helps to limit iron-catalyzed free radical damage (*1*). The intracellular location of ferritin varies from mostly cytosolic in vertebrates (*2*−*4*) to entirely vacuolar in many insects (*5*, *6*), while it is limited to chloroplasts in plants (*7*). Mitochondria process large amounts of iron through the iron−sulfur cluster and heme biosynthetic pathways, and thus, iron homeostasis is particularly important in these organelles (*8*). A ferritin targeted to mitochondria has been identified, but its mammalian origin and limited tissue distribution (*9*) suggest that additional general mechanisms of mitochondrial iron regulation may be present. A growing body of evidence points at the mitochondrial matrix protein, frataxin, as an early and highly conserved mechanism (reviewed in ref *8*).

Frataxin homologues are found in α-purple bacteria and most eukaryotes (*10*), and the human homologue is widely expressed, particularly in tissues with high-energy requirements (*11*). Frataxin-depleted yeast variants show loss of iron−sulfur cluster-containing enzymes, mitochondrial iron accumulation, and increased oxidative damage to both mitochondrial and nuclear DNA (*12*−*14*). Similar findings have been reported for mouse frataxin knockout mutants (*15*) as well as tissues and cell lines derived from patients with

† H.N. was supported by a fellowship from the Government of Saskatchewan and the College of Medicine of the University of Saskatchewan. SSRL is funded by the Department of Energy, Office of Basic Energy Sciences, under Contract DE-AC03-76SF00515. The SSRL Structural Molecular Biology Program is supported by the National Institutes of Health, National Center for Research Resources, Biomedical Technology Program, and the Department of Energy, Office of Biological and Environmental Research. This work was supported in part by research grants from the Canadian Institutes for Health Research (to H.N.), Grant AG15709 from the National Institute on Aging, National Institutes of Health, and a grant from the Muscular Dystrophy Association (to G.I.). H.A.O. is supported by Fellowship NRSA 44748 from the National Institute of Neurological Disorders and Stroke, National Institutes of Health.

* To whom correspondence should be addressed. H.N.: Department of Anatomy and Cell Biology, College of Medicine, University of Saskatchewan, A315 Health Sciences Bldg., 107 Wiggins Rd., Saskatoon, SK, Canada S7N 5E5; e-mail, h.nichol@usask.ca; phone, (306) 966-4075; fax, (306) 966-4298. G.I.: Mayo Clinic and Foundation, 200 First St. SW, Stabile 7-52, Rochester, MN 55905; e-mail, isaya@mayo.edu; phone, (507) 266-0110; fax, (507) 266-9315.

‡ University of Saskatchewan.

§ Mayo Clinic and Foundation.

|| Stanford Synchrotron Radiation Laboratory.

10.1021/bi027021l CCC: $25.00
Published on Web 05/02/2003

Friedreich ataxia, an autosomal recessive neurodegenerative disease caused by frataxin deficiency (*8*). The biochemical alterations associated with frataxin defects can be explained by recent reports demonstrating that yeast frataxin is required for the biogenesis of iron−sulfur clusters (*16*−*18*), the lack of which is known to derange mitochondrial iron homeostasis (*19*).

The mechanism of frataxin has been analyzed *in vitro* via the use of purified full-length forms of the protein. Yeast frataxin is activated by Fe(II) in the presence of atmospheric O_2 and forms an oligomer, α_3, with ferroxidase activity [$2Fe(II) + O_2 + 2H^+ \rightarrow 2Fe(III) + H_2O_2$] (*20*). When the Fe(II) concentration exceeds that of the ferroxidase sites on the protein [Fe(II)/mYfh1p > 0.5], autoxidation [$4Fe(II) + O_2 + 4H^+ \rightarrow 4Fe(III) + 2H_2O$] overcomes ferroxidation (*20*). Moreover, at iron concentrations that exceed the capacity of α_3, stepwise assembly of trimers yields a 48-subunit multimer of 840 kDa that accumulates ∼50 atoms of iron per subunit (*21*, *22*). Unlike yeast frataxin, the human homologue assembles during expression in *Escherichia coli*, forming individual particles of ∼1 MDa and rod-shaped polymers of these particles (*23*). Upon purification from bacterial cells, the assembled human protein contains low iron levels (0.1−0.3 atom per subunit) but exhibits ferroxidase activity and can be loaded with ∼10 atoms of iron per subunit (ref *23* and unpublished results). This behavior is similar to that described for recombinant ferritins that polymerize during expression in *E. coli* (*24*−*26*), forming a hollow sphere of 24 subunits with a capacity of up to 187 atoms of iron per subunit. Ferrous cations pass through channels between the subunits and are oxidized to Fe(III) either at diiron ferroxidase sites on the protein or directly at the surface of the growing ferritin core (*27*). Thus, the yeast frataxin iron core appears to grow through the sequential addition of trimer-bound ferric iron moieties, while the human frataxin iron core, like ferritin, forms within a preassembled homopolymer. In electron micrographs, however, the iron associated with both yeast and human frataxin polymers appears as small electron-dense granules of ∼2−4 nm, severalfold smaller than the iron core of ferritin (*22*, *23*). Previous analyses of ferritin iron cores by extended X-ray absorption fine structure (EXAFS) and Mössbauer spectroscopies indicate a resemblance to natural inorganic ferrihydrite (*28*−*33*). Here we use high-resolution EXAFS spectroscopy to provide the first detailed structural information for the iron core of yeast and human frataxin, and compare the frataxin and ferritin iron cores.

MATERIALS AND METHODS

Preparation of Iron-Loaded Yeast and Human Frataxin. Expression and purification of the mYfh1p monomer and the human frataxin polymer were carried out as described previously (*22*, *23*). The iron-loaded mYfh1p multimer was prepared as described previously (*22*) with the modifications noted below. A 40 μM solution of the mYfh1p monomer was incubated with 40 equiv of ferrous iron in 10 mM HEPES-KOH (pH 7.4) [HEPES (pH 7.4)] for 1 h at 30 °C (total volume of 30 mL). The sample was concentrated to 1 mL, centrifuged for 5 min at 20800*g*, and loaded onto an HR16/60 Sephacryl 300 column (Amersham Pharmacia Biotech). The protein was eluted with 125 mL of 10 mM HEPES (pH 7.4) and 100 mM NaCl (HN100) at a flow rate 0.6 mL/min, and fractions containing the multimer were pooled (∼7 mL) and concentrated to 100 μL. Iron loading of horse spleen apoferritin (Sigma) was carried out as described by others (*25*). The sample was treated in a manner similar to that for the mYfh1p multimer except that it was purified through an HR16/50 Superdex 200 column (Amersham Pharmacia Biotech). Samples from two consecutive purification procedures were pooled and analyzed for protein concentration by SDS−PAGE and Coomassie blue staining, and for iron concentration by inductively coupled plasma emission spectroscopy. X-ray absorption spectroscopy was performed on three sample sets. The iron concentration was 78−130 mM with an Fe/subunit ratio of ∼43−47/1 in two independent mYfh1p preparations, and 104 mM with an Fe/subunit ratio of ∼69/1 in one ferritin preparation. To measure in transmittance, highly concentrated samples were prepared in 20% glycerol with iron concentrations for mYfh1p and ferritin of 316 and 348 mM, respectively. A 33.5 μM solution of the human frataxin polymer was incubated with 10 equiv of ferrous iron in 10 mM HEPES-KOH (pH 7.0) [HEPES (pH 7.0)] for 10 h at room temperature (total volume of 10 mL). After addition of 1% glycerol, this sample was concentrated to a volume of 1 mL in a centrifugal filter device (Amicon Ultra, 100 kDa molecular mass cutoff, Millipore), diluted 10-fold with HEPES (pH 7.0) and 1% glycerol, and concentrated again to a volume of 1 mL. This process was repeated three times to minimize the amount of residual free iron, and the sample was eventually concentrated to a final volume of 150 μL. The iron concentration was 15 mM with an Fe/subunit ratio of ∼7/1.

XAS Samples for X-ray Fluorescence. Iron-loaded mYfh1p multimer samples were prepared for X-ray absorption spectroscopy by dilution of the sample to a final concentration of 20 mM iron in HEPES (pH 7.4), and glycerol was added to a final concentration of 20% to reduce ice diffraction artifacts. Human frataxin was analyzed at a final iron concentration of 10 mM in HEPES (pH 7.0) and 10% glycerol. Samples were loaded into 1 mm path length Lucite sample cells and flash-frozen in cold isopentane.

XAS Samples for Transmittance. Highly concentrated mYfh1p multimer and horse spleen holoferritin were prepared in 20% glycerol, flash-frozen immediately after preparation as described above, and then shipped to Stanford Synchrotron Radiation Laboratory (SSRL) on dry ice. An aqueous slurry of two-line ferrihydrite was loaded into a Lucite sample cell as described above. Other iron model compounds were intimately ground with a boron nitride diluent and compressed between layers of Mylar in a 2 mm thick sample holder.

X-ray Absorption Spectroscopy. Data were acquired at SSRL with the SPEAR storage ring containing 60−100 mA at 3.0 GeV, using 1.8 T wiggler beamline 7-3 with a Si(220) double-crystal monochromator. The monochromator vertical entrance aperture was adjusted to 1 mm to optimize energy resolution. Harmonic rejection was accomplished by detuning one monochromator crystal to approximately 50% off peak, and no focusing optics were in the beamline. The incident X-ray intensity was monitored using an N_2-filled ionization chamber. For ferritin and frataxin, the X-ray absorption spectra were recorded as Fe Kα fluorescence excitation spectra using an array of 30 germanium detectors or in transmittance mode using N_2-filled ionization chambers

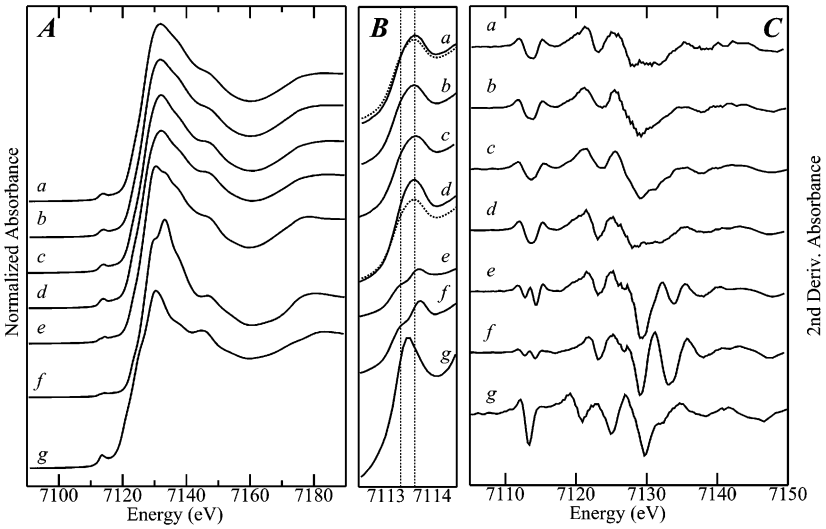

FIGURE 1: Near-edge spectra of the iron K-edges (A), pre-edge feature (B), and corresponding polynomial-smoothed second derivative (C) of (a) horse spleen ferritin, (b) yeast frataxin, (c) human frataxin, (d) synthetic two-line ferrihydrite, (e) hematite, (f) goethite, and (g) synthetic magnetite. (A) The near edges of yeast and human frataxin are very similar to those of ferritin and less similar to those of two-line ferrihydrite. (B) The yeast frataxin pre-edge feature (dashed line) is overlaid on that of ferritin to show similarity and that of two-line ferrihydrite to show differences. The pre-edge features of frataxin, ferritin, and ferrihydrite show the decreased intensity and peak maximum (7114 eV) that are characteristic of ferric iron octahedrally coordinated to oxygen. Minerals with mixed ferrous and ferric iron, such as magnetite (g), have high-intensity pre-edge features with peak maxima at ~7113 eV. (C) The second derivatives were calculated by least-squares fitting a third-order polynomial around a 1 eV range. The second derivatives show a few, subtle differences between frataxin and ferritin. All edges were collected in transmittance mode with the exception of that of human frataxin.

on either side of the sample to monitor absorbance. Model compounds were measured in transmittance mode. Samples were kept between 5 and 10 K in an Oxford Instruments liquid helium flow cryostat, and the X-ray energy was calibrated with reference to the lowest-energy inflection point of a metallic iron foil standard that was assumed to be 7111.3 eV. Data for two independent yeast frataxin samples (not shown) and one ferritin sample were collected in fluorescence mode and analyzed. Between seven and twelve 35 min scans were accumulated for each yeast frataxin sample. Because of the lower iron concentration of human frataxin, 18 scans were accumulated to a k of 16 Å^{-1}. Data for highly concentrated yeast frataxin and ferritin were collected in transmittance mode to a k of 18 Å^{-1} and analyzed. An improved signal-to-noise ratio permitted resolution of one additional Fe−O shell. Multiple scattering interactions seen in ferritin that had been aged for 2 weeks were not seen in ferritin or frataxin that was frozen immediately after iron loading.

XAS Data Analysis. The extended X-ray absorption fine structure (EXAFS) oscillations $\chi(k)$ were analyzed using the EXAFSPAK suite of computer programs. *Ab initio* theoretical phase and amplitude functions were generated with FEFF version 7.2 (*34*, *35*). No smoothing or related data manipulations were performed.

RESULTS

Fe K Near-Edge X-ray Absorption Spectra. Iron K near edge spectra of ferritin and frataxin iron cores are compared with those of other biominerals in Figure 1. The spectra of ferritin (Figure 1A, a) and yeast and human frataxin (Figure 1A, b and c) are nearly identical to each other and slightly different from the spectrum of two-line ferrihydrite (Figure 1A, d). The small pre-edge features at ~7113.5 eV are the formally dipole-forbidden, quadrupole-allowed 1s → 3d transitions (*36*). For individual iron sites, this transition shows structure related to the electronic structure of the iron, and specifically to the 3d manifold (*37*, *38*). In centrosymmetric (e.g., octahedral) environments, two quadrupole-allowed transitions are observed [1s → 3d(t_{2g}) and 1s → 3d(e_g)], but in noncentrosymmetric (e.g., tetrahedral) environments, mixing of the 4p and e levels occurs, resulting in significant dipole-allowed intensity for this transition (e.g., magnetite, Figure 1, g). The 1s → 3d feature is thus an excellent probe of electronic structure, and can be used to discriminate high-spin from low-spin ferric species, and detect the presence of mixed ferrous and ferric species (*37*, *38*). The shape and intensity of the pre-edge features of human and yeast frataxin (Figure 1B) are nearly identical to those of ferritin but different from those of two-line ferrihydrite (Figure 1B), indicating closely related metal sites in frataxin and ferritin, and suggest the presence of high-spin ferric octahedral iron (*39*, *40*). The second-derivative plot (Figure 1C) shows only subtle differences in the spectra of yeast frataxin and ferritin collected in transmittance mode and the spectra of human frataxin collected in fluorescence mode. We conclude that frataxin iron cores are composed of ferric iron coordinated with six oxygen atoms with no indication of significant levels of ferrous species.

EXAFS Spectroscopy. The EXAFS and EXAFS Fourier transforms of highly concentrated yeast frataxin and ferritin iron cores and the more dilute human frataxin are shown in Figure 2, together with the results of the curve-fitting analysis. EXAFS-derived coordination numbers and Fe−Fe distances can be used to distinguish different iron minerals (*41*). The EXAFS of human and yeast frataxin can be overlaid and are identical within the noise (data not shown) and therefore will be discussed together as frataxin. Ferritin and frataxin exhibit very similar Fe−O and Fe−Fe interactions (Figure 2 and Table 1) that are also similar to those of

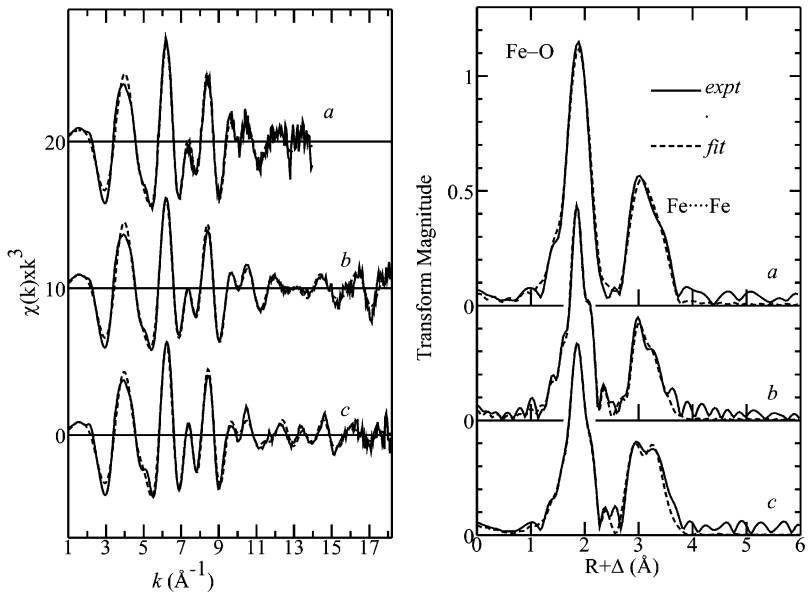

FIGURE 2: Iron K-edge EXAFS spectra and corresponding EXAFS Fourier transforms of iron cores of human frataxin (fluorescence mode to a k of 14 Å^{-1}) (a), yeast frataxin (b), and horse spleen ferritin (c) (transmittance mode to a k of 18 Å^{-1}). Solid lines show experimental data, while the dashed lines show the best fits. The EXAFS Fourier transforms have been phase-corrected for the Fe−O backscattering. EXAFS data were collected with a point spacing of 0.05 and a count time varying between 2 and 16 s (proportional to k^2) for $k = 18$ Å^{-1} data and between 2 and 12 s for $k = 12$ Å^{-1} data.

Table 1: EXAFS Curve-Fitting Results[a]

	yeast frataxin				human frataxin				horse spleen ferritin			
	N	*R*	σ^2	error[b]	*N*	*R*	σ^2	error[b]	*N*	*R*	σ^2	error[b]
Fe−O	2.9	1.939(1)	0.003(1)	0.0047	3	1.929(1)	0.005(1)	0.0063	3.3	1.940(1)	0.005(1)	0.0054
Fe−O	2.6	2.072(1)			3	2.049(1)			2.5	2.075(2)		
Fe−O	0.6	2.253(2)							0.5	2.277(3)		
Fe−Fe	0.4	2.963(2)	0.005(1)		0.4	2.950(2)	0.003(1)		1.0	2.987(2)	0.003(1)	
Fe−Fe	1.2	3.075(2)			1.0	3.068(1)			0.9	3.107(1)		
Fe−Fe	0.5	3.453(1)			0.6	3.452(2)			0.6	3.455(2)		

[a] Coordination number, *N*, interatomic distance, *R* (Å), and (thermal and static) mean-square deviation in *R* (the Debye−Waller factor), σ^2 (Å^2). A combined single σ^2 was used for Fe−O and Fe−Fe. *N* was determined independently for each shell using a two-parameter search algorithm. For ferritin, yeast frataxin, and human frataxin, the threshold shifts, ΔE_0, were −8.8, −8.7, and −10.3, respectively. Values in parentheses are the estimated standard deviations (precisions) obtained from the diagonal elements of the covariance matrix. The accuracies will always be somewhat larger than the precisions, typically ±0.02 Å for *R* and ±20% for *N* and σ^2. Note that EXAFS cannot readily distinguish between scatterers with similar atomic numbers such as nitrogen and oxygen. [b] The fit error is defined as $[\sum k^6(\chi_{exptl} - \chi_{calcd})^2/\sum k^6\chi_{exptl}^2]^{1/2}$.

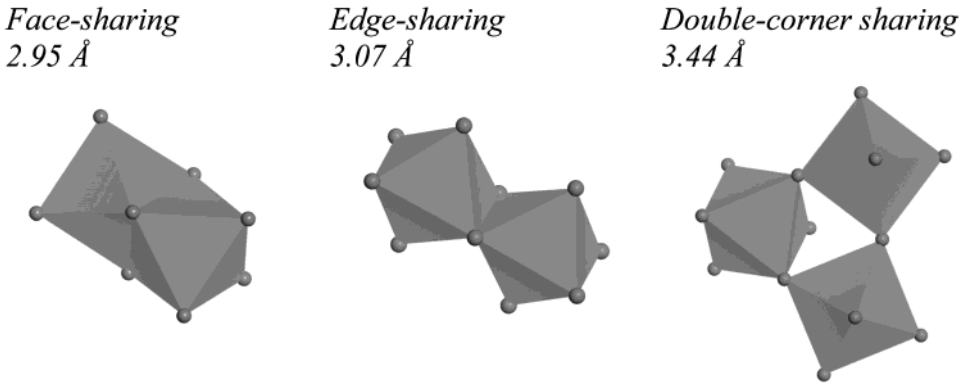

FIGURE 3: Alternative methods of linking FeO_6 octahedra, showing face-sharing, edge-sharing, and double corner-sharing structures.

six-line ferrihydrite (*41*). Because of the extended k range of our transmittance data, three discrete Fe−O/OH interactions were resolved within the range expected for octahedrally coordinated iron (Table 1). Some variation in the apparent coordination numbers *N* for these Fe−O interactions was observed between frataxin and ferritin, but this is probably close to the accuracy for *N*, and may not be significant. The Fe−Fe distances can be used to discriminate the arrangement of adjacent FeO_6 octahedra. In ferrihydrite minerals, distances of 2.95, 3.05, and 3.44 Å are typical of face-sharing, edge-sharing, and double corner-sharing octahedra, respectively (*41*) (see Figure 3). The ratio of edge-sharing to double corner-sharing interactions indicates that frataxin cores are more similar to six-line than to two-line ferrihydrite (*41*). The presence of significant face-sharing interactions in the frataxin EXAFS leads us to conclude that

the core can best be modeled as an agglomeration of locally ordered fragments that resemble six-line ferrihydrite. As ferrihydrite ages, the proportions of face-, edge-, and double corner-sharing interactions change (*42*). In ferritin samples that were aged, the EXAFS Fourier transform exhibited a peak at ~6 Å (data not shown). Observation of such long-range interactions is unusual, especially in biological materials, and when seen, it is often due to multiple scattering from approximately collinear arrangements of atoms. The development of such long-range order may be related to age-related core condensation.

DISCUSSION

We have shown that yeast and human frataxin assemble iron cores that are identical to each other and closely resemble but are distinct from the horse spleen ferritin iron core (*41*). Frataxin and ferritin cores have similar Fe−O coordination, with the range characteristic of octahedral coordination, and their near-edge spectra are consistent with octahedrally coordinated ferric sites. Iron−iron distances and their relative proportions can be used to identify various iron oxide minerals with precision (*41*). Frataxin iron cores show the Fe−Fe interactions characteristic of six-line ferrihydrite, with face-sharing interactions and a relatively high proportion of double corner-sharing interactions indicating a level of order higher than that seen in amorphous ferrihydrite. Nevertheless, the ferrihydrite in frataxin is less condensed and well ordered than ferritin, having fewer face-sharing Fe−Fe interactions.

Our results provide clues that may help to explain how frataxin iron cores form *in vitro*. EXAFS data support the conclusion that frataxin iron cores result from the aggregation of small ferrihydrite crystallites as they do not have the degree of order of the ferritin iron core (*41*). An alternative interpretation of our EXAFS data is that differences in face-sharing Fe−Fe interactions between frataxin and ferritin cores reflect the larger size and smaller surface-to-volume ratio of the ferritin cores (*22*, *23*). Current models suggest that ferrihydrite grows by the assembly of chains of dioctahedra linked by edge-sharing interactions, with corner-sharing interactions appearing only after chains have formed (*41*, *43*). The small size of the frataxin cores (*22*, *23*) would appear to limit the absolute number of interactions between chains of octahedra.

We favor the first interpretation because it is compatible with the different modes of iron loading of yeast and human frataxin. The binding and oxidation of Fe(II) occur concomitantly with protein assembly in the case of yeast frataxin (*20*, *21*) but within the preassembled homopolymer in the case of human frataxin (*23*). Although the mechanism by which human frataxin assembles during expression in *E. coli* is still unknown, ongoing electrode oximetry studies indicate that the human frataxin polymer has ferroxidase activity, with probably three subunits forming one ferroxidation site as described for yeast frataxin (*20*). We speculate that frataxin iron cores form in accord with the model proposed for bacterial biomineralization (*44*). At physiologic pH, ferric oxy−hydroxy species have a low solubility and tend to form very small solid phase particles that aggregate at negatively charged surfaces (*44*), such as can be found on frataxin (*45*). During bacterial biomineralization, as ferrihydrite microcrystals align, their free surfaces are eliminated, resulting in a reduction in surface free energy (*44*, *46*). The alignment and binding of one microcrystal to another depend on concentration, and are thought to occur through random interactions (*44*). Both yeast and human frataxin bind and catalyze oxidation of Fe(II) to Fe(III) (ref *20* and unpublished results) and may further facilitate the aggregation of small ferrihydrite particles at the surface of their acidic patches. The alignment and binding of one microcrystal to another may be facilitated by the interaction of trimers as the yeast frataxin polymer assembles (*20*). Similarly, human frataxin may guide biomineralization by keeping the ferric iron microcrystallites in a soluble form and at a high concentration within the assembled protein. According to this model, biomineralization is an integral part of the assembly process of yeast frataxin, whereas in human frataxin, biomineralization occurs after protein assembly. However, the biomineral that forms is the same, consistent with previous complementation studies showing that yeast and human frataxin are functional homologues (*47*, *48*). The mechanism used by human frataxin results in a lower iron loading capacity (10 vs 50 Fe atoms/subunit) but would appear to provide a faster means of sequestering excess iron in a protein-protected compartment. The iron loading capacity of frataxin may not be as critical for human cells that unlike *Saccharomyces cerevisiae* also possess cytoplasmic and mitochondrial ferritins.

Our results are consistent with a direct role of frataxin in mitochondrial iron metabolism. In the yeast *S. cerevisiae*, a reduced level of expression of frataxin severely limits iron sulfur cluster assembly but has a less dramatic effect on heme biosynthesis (*17*, *49*). Similarly, marked deficiencies of iron−sulfur cluster-containing enzymes (*50*) but only a relatively small heme deficiency (*51*) have been detected in Friedreich's ataxia patients. Thus, frataxin may primarily be part of mechanisms that deal with iron flux through the iron−sulfur cluster biosynthetic pathway. Mitochondrial ferritin, which is overexpressed in erythroblasts of patients with sideroblastic anemia (*9*), may have evolved more recently to deal with the large flux of iron required for heme biosynthesis in erythroid cells (*52*). Interestingly, human frataxin expression is repressed during erythroid differentiation (*53*), suggesting a regulatory mechanism for increasing iron flux through the heme pathway by limiting synthesis of iron−sulfur clusters. Thus, distinct and differentially regulated iron storage proteins may be required for adequate regulation of mitochondrial iron utilization in different organisms and cell types.

ACKNOWLEDGMENT

Minerals used in the preparation of some iron models were a kind gift from Prof. Gordon Brown (Stanford University). We are indebted to Dr. Hugh Harris for assistance in data acquisition. We also thank Sungjo Park for helpful discussions.

REFERENCES

1. Harrison, P. M., and Arosio, P. (1996) *Biochim. Biophys. Acta 1275*, 161−203.
2. Richter, G. W. (1978) *Am. J. Pathol. 91*, 363−396.
3. Renaud, D. L., Nichol, H., and Locke, M. (1991) *J. Submicrosc. Cytol. Pathol. 23*, 501−507.

4. Thompson, K. J., Fried, M. G., Ye, Z., Boyer, P., and Connor, J. R. (2002) *J. Cell Sci. 115*, 2165−2177.
5. Nichol, H. K., and Locke, M. (1990) *Tissue Cell 22*, 767−777.
6. Nichol, H., Law, J. H., and Winzerling, J. J. (2002) *Annu. Rev. Entomol. 47*, 535−559.
7. Briat, J. F., Lobreaux, S., Grignon, N., and Vansuyt, G. (1999) *Cell. Mol. Life Sci. 56*, 155−166.
8. Rotig, A., Sidi, D., Munnich, A., and Rustin, P. (2002) *Trends Mol. Med. 8*, 221−224.
9. Levi, S., Corsi, B., Bosisio, M., Invernizzi, R., Volz, A., Sanford, D., Arosio, P., and Drysdale, J. (2001) *J. Biol. Chem. 276*, 24437−24440.
10. Musco, G., Stier, G., Kolmerer, B., Adinolfi, S., Martin, S., Frenkiel, T., Gibson, T., and Pastore, A. (2000) *Struct. Folding Des. 8*, 695−707.
11. Campuzano, V., Montermini, L., Molto, M. D., Pianese, L., Cossee, M., Cavalcanti, F., Monros, E., Rodius, F., Duclos, F., Monticelli, A., et al. (1996) *Science 271*, 1423−1427.
12. Babcock, M., de Silva, D., Oaks, R., Davis-Kaplan, S., Jiralerspong, S., Montermini, L., Pandolfo, M., and Kaplan, J. (1997) *Science 276*, 1709−1712.
13. Foury, F., and Cazzalini, O. (1997) *FEBS Lett. 411*, 373−377.
14. Karthikeyan, G., Lewis, L. K., and Resnick, M. A. (2002) *Hum. Mol. Genet. 11*, 1351−1362.
15. Puccio, H., Simon, D., Cossee, M., Criqui-Filipe, P., Tiziano, F., Melki, J., Hindelang, C., Matyas, R., Rustin, P., and Koenig, M. (2001) *Nat. Genet. 27*, 181−186.
16. Foury, F. (1999) *FEBS Lett. 456*, 281−284.
17. Muhlenhoff, U., Richhardt, N., Ristow, M., Kispal, G., and Lill, R. (2002) *Hum. Mol. Genet. 11*, 2025−2036.
18. Duby, G., Foury, F., Ramazzotti, A., Herrmann, J., and Lutz, T. (2002) *Hum. Mol. Genet. 11*, 2635−2643.
19. Muhlenhoff, U., and Lill, R. (2000) *Biochim. Biophys. Acta 1459*, 370−382.
20. Park, S., Gakh, O., Mooney, S. M., and Isaya, G. (2002) *J. Biol. Chem. 277*, 38589−38595.
21. Adamec, J., Rusnak, F., Owen, W. G., Naylor, S., Benson, L. M., Gacy, A. M., and Isaya, G. (2000) *Am. J. Hum. Genet. 67*, 549−562.
22. Gakh, O., Adamec, J., Gacy, A. M., Twesten, R. D., Owen, W. G., and Isaya, G. (2002) *Biochemistry 41*, 6798−6804.
23. Cavadini, P., O'Neill, H. A., Benada, O., and Isaya, G. (2002) *Hum. Mol. Genet. 11*, 217−227.
24. Hudson, A. J., Andrews, S. C., Hawkins, C., Williams, J. M., Izuhara, M., Meldrum, F. C., Mann, S., Harrison, P. M., and Guest, J. R. (1993) *Eur. J. Biochem. 218*, 985−995.
25. Levi, S., Salfeld, J., Franceschinelli, F., Cozzi, A., Dorner, M. H., and Arosio, P. (1989) *Biochemistry 28*, 5179−5184.
26. Rucker, P., Torti, F. M., and Torti, S. V. (1997) *Protein Eng. 10*, 967−973.
27. Chasteen, N. D., and Harrison, P. M. (1999) *J. Struct. Biol. 126*, 182−194.
28. Joo, M. S., Tourillon, G., Sayers, D. E., and Theil, E. C. (1990) *Biol. Met. 3*, 171−175.
29. Mansour, A. N., Thompson, C., Theil, E. C., Chasteen, N. D., and Sayers, D. E. (1985) *J. Biol. Chem. 260*, 7975−7979.
30. Yang, C. Y., Bryan, A. M., Theil, E. C., Sayers, D. E., and Bowen, L. H. (1986) *J. Inorg. Biochem. 28*, 393−405.
31. Rohrer, J. S., Islam, Q. T., Watt, G. D., Sayers, D. E., and Theil, E. C. (1990) *Biochemistry 29*, 259−264.
32. Hwang, J., Krebs, C., Huynh, B. H., Edmondson, D. E., Theil, E. C., and Penner-Hahn, J. E. (2000) *Science 287*, 122−125.
33. Moenne-Loccoz, P., Krebs, C., Herlihy, K., Edmondson, D. E., Theil, E. C., Huynh, B. H., and Loehr, T. M. (1999) *Biochemistry 38*, 5290−5295.
34. Mustre de Leon, J., Rehr, J. J., Zabinsky, S. I., and Albers, R. C. (1991) *Phys. Rev. B: Condens. Matter Mater. Phys. 44*, 4146−4156.
35. Rehr, J. J., Mustre de Leon, J., Zabinsky, S. I., and Albers, R. C. (1991) *J. Am. Chem. Soc. 113*, 5135−5140.
36. Shulman, R. G., Yafet, Y., Eisenberger, P., and Blumberg, W. E. (1976) *Proc. Natl. Acad. Sci. U.S.A. 73*, 1384−1388.
37. Westre, T. E., Kennepohl, P., deWitt, J., Hedman, B., Hodgson, K. O., and Solomon, E. I. (1997) *J. Am. Chem. Soc. 119*, 6297−6314.
38. Wilke, M., Farge, F., Petit, P.-E., Brown, G. E., and Martin, F. (2001) *Am. Mineral. 86*, 714−730.
39. Ikeda-Saito, M., Hori, H., Andersson, L. A., Prince, R. C., Pickering, I. J., George, G. N., Sanders, C. R., Jr., Lutz, R. S., McKelvey, E. J., and Mattera, R. (1992) *J. Biol. Chem. 267*, 22843−22852.
40. Shiro, Y., Sato, F., Suzuki, T., Iizuka, T., Matsushita, T., and Oyanagi, H. (1990) *J. Am. Chem. Soc. 112*, 2921−2924.
41. Drits, V. A., Sakharov, B. A., Salyn, A. L., and Manceau, A. (1993) *Clay Miner. 28*, 185−207.
42. Waychunas, G. A., Rea, B. A., Fuller, C. C., and Davis, J. A. (1993) *Geochim. Cosmochim. Acta 57*, 2251−2269.
43. Manceau, A., and Drits, V. A. (1993) *Clay Miner. 28*, 165−184.
44. Banfield, J. F., Welch, S. A., Zhang, H., Ebert, T. T., and Penn, R. L. (2000) *Science 289*, 751−754.
45. Dhe-Paganon, S., Shigeta, R., Chi, Y. I., Ristow, M., and Shoelson, S. E. (2000) *J. Biol. Chem. 275*, 30753−30756.
46. Penn, R. L., and Banfield, J. F. (1998) *Science 281*, 969−971.
47. Wilson, R. B., and Roof, D. M. (1997) *Nat. Genet. 16*, 352−357.
48. Cavadini, P., Gellera, C., Patel, P. I., and Isaya, G. (2000) *Hum. Mol. Genet. 9*, 2523−2530.
49. Lesuisse, E., Santos, R., Matzanke, B. F., Knight, A. A. B., Camadro, J. M., and Dancis, A. (2003) *Hum. Mol. Genet. 12*, 879−889.
50. Rotig, A., de Lonlay, P., Chretien, D., Foury, F., Koenig, M., Sidi, D., Munnich, A., and Rustin, P. (1997) *Nat. Genet. 17*, 215−217.
51. Morgan, R. O., Naglie, G., Horrobin, D. F., and Barbeau, A. (1979) *Can. J. Neurol. Sci. 6*, 227−232.
52. Ponka, P. (1997) *Blood 89*, 1−25.
53. Becker, E. M., Greer, J. M., Ponka, P., and Richardson, D. R. (2002) *Blood 99*, 3813−3822.

BI027021L